Nonlinear elasticity of wrinkled atomically thin membranes

Sarafraz, Ali; Arjmandi-Tash, Hadi; Dijkink, Laura; Sajadi, Banafsheh; Moeini, Mohsen; Steeneken, Peter G.; Alijani, Farbod

DOI
10.1063/5.0061822

Publication date
2021

Document Version
Final published version

Published in
Journal of Applied Physics

Citation (APA)
Sarafraz, A., Arjmandi-Tash, H., Dijkink, L., Sajadi, B., Moeini, M., Steeneken, P. G., & Alijani, F. (2021). Nonlinear elasticity of wrinkled atomically thin membranes. *Journal of Applied Physics*, *130*(18), Article 184302. https://doi.org/10.1063/5.0061822

Journal of Applied Physics

Nonlinear elasticity of wrinkled atomically thin membranes

Cite as: J. Appl. Phys. **130**, 184302 (2021); https://doi.org/10.1063/5.0061822
Submitted: 30 June 2021 • Accepted: 21 October 2021 • Published Online: 11 November 2021

Ali Sarafraz, Hadi Arjmandi-Tash, Laura Dijkink, et al.

Journal of Applied Physics ARTICLE scitation.org/journal/jap

Nonlinear elasticity of wrinkled atomically thin membranes

Cite as: J. Appl. Phys. **130**, 184302 (2021); doi: 10.1063/5.0061822
Submitted: 30 June 2021 · Accepted: 21 October 2021 ·
Published Online: 11 November 2021 · Corrected: 12 November 2021

Ali Sarafraz,[1,a)] Hadi Arjmandi-Tash,[1] Laura Dijkink,[1] Banafsheh Sajadi,[1,b)] Mohsen Moeini,[2] Peter G. Steeneken,[1,3] and Farbod Alijani[1,c)]

AFFILIATIONS

[1]Department of Precision and Microsystems Engineering, Faculty of Mechanical, Maritime and Materials Engineering, Delft University of Technology, 2628 CD Delft, The Netherlands
[2]Mechanical Engineering Department, Amirkabir University of Technology, P.O. Box 15875-4413 Tehran, Iran
[3]Kavli Institute of Nanoscience, Faculty of Applied Sciences, Delft University of Technology, 2628 CJ Delft, The Netherlands

[a)]**Author to whom correspondence should be addressed:** a.sarafraz@tudelft.nl
[b)]**Also at:** Amber Implants BV, Prinses Margrietplantsoen 33, 2595 AM, The Hague, The Netherlands
[c)]**Electronic mail:** f.alijani@tudelft.nl

ABSTRACT

Owing to their atomic thickness and low bending rigidity, suspended two-dimensional (2D) materials are prone to wrinkle formation. Here, we use molecular dynamics (MD) simulations to probe the effect of these wrinkles on the nonlinear elasticity of atomically thin graphene membranes. We observe a stress–strain response that consists of two linear regions that are separated by a transition. It is found that this transition is sharp in membranes where wrinkles are formed by uneven stresses at the boundaries. However, when wrinkles are formed by crystal defects, this nonlinear transition is seen to be more gradual. To capture these effects, we use a phenomenological model based on experimentally measurable quantities. We demonstrate the model's fidelity by fitting it to the MD simulated nonlinear response of many graphene membranes providing evidence that the sharpness of the transition between the linear regions in the stress–strain response is a measure of the type of wrinkles and can be quantified by our model.

I. INTRODUCTION

Wrinkles are out-of-plane deviations from flat configuration that are frequently observed in the fabrication of 2D material membranes. These corrugations manifest themselves in both suspended[1] and substrate-supported[2,3] 2D materials and can significantly influence their electronic and mechanical properties.[4–6] Therefore, thorough understanding of the influence of wrinkles in 2D material membranes is key to the development of high-performance 2D nanomechanical devices.

Multiple wrinkled regions with different patterns may coexist in a single 2D membrane.[7–13] These regions often comprise static wrinkles that can be the consequence of uneven stress at the boundaries of the membrane,[10,14,15] surface functionalization with molecules,[16–18] or crystal defects.[19,20] Among them, the latter is particularly shown to reduce the stiffness of 2D membranes and lead to auxetic properties such as negative Poisson's ratio.[21] Entropic fluctuations due to Brownian motion are another source of wrinkles intrinsic to these materials that can give rise to exotic properties such as negative thermal expansion coefficient[22] and size-dependent elastic constants.[23,24]

The stretching of a wrinkled 2D material is a two-level process and exhibits a bilinear stress–strain response that consists of two linear parts, each with a different effective stiffness. At relatively low tensile strains, the applied force "irons out" the wrinkles and results in low effective stiffness.[25] Once the wrinkles are suppressed, high stiffness is observed due to the stretching of the atomic bonds.[26] Recent experimental observations also suggest a nonlinear transition state between these two stiffness levels that so far is not well-understood.[10,25,26]

This work aims at clarifying the nature of this nonlinear behavior via molecular dynamics (MD) simulations. We perform our simulations on graphene as a model system to develop a

general procedure for probing the elasticity of wrinkled 2D materials. We create wrinkles both by compressive forces at the boundaries and by introducing crystal defects. While pre-stress is the root cause of wrinkle formation in the presence of compressive forces at the boundaries, 2D crystal defects in a stress-free membrane generate a wrinkled state that is solely the result of the 2D lattice imperfections.

The proposed approach for probing the nonlinear elasticity of wrinkled graphene is as follows: In Sec. II, we use a theoretical model to qualitatively describe the nonlinear elasticity of wrinkled membranes. In Sec. III, we employ MD simulations for modelling and comparing the response of membranes that are either wrinkled by compressive forces at the boundaries or by crystal defects. Finally, in Sec. IV, we discuss the effects of these wrinkles on the stress–strain response of graphene and propose a phenomenological model that captures the nonlinear elasticity of wrinkled membranes and identifies the differences between the effect of lattice defects and compressive stress via the stress–strain response.

II. ANALYTICAL MODELING

From linear elasticity, it is known that isotropic materials follow Hooke's law. According to this law, material stiffness is characterized by the biaxial modulus $E^f_{2D} = Eh/(1-\nu)$ (E is Young's modulus, ν is Poisson's ratio, and h is the thickness) in a standard equi-biaxial test. However, for wrinkled membranes, experimental results show that the stress–strain response deviates from Hooke's law, and the observed slopes do not depend on the *material stiffness* but instead are *geometrical effects* that can be influenced by the boundary forces and morphological imperfections.[27]

In order to model such effects in a simple way, we assume Hooke's law for the material, use plane-stress condition, and determine the engineering strain ε in the following way:[10]

$$\varepsilon(\sigma) = \frac{1}{E^f_{2D}}\sigma + \frac{1}{2}\frac{\Delta A(\sigma)}{A}, \tag{1}$$

where σ is the engineering stress, A is the surface area of the flat lattice in the absence of external forces, and ΔA is the "hidden area" that is defined as the difference between the total surface area of the membrane and the area projected onto the plane containing the boundaries. Unlike equi-biaxial straining of a flat membrane that solely yields in-plane stretching, the straining of a wrinkled membrane involves in-plane stretching and out-of-plane bending, simultaneously. Thus, Eq. (1) has an additional term with respect to conventional linear Hooke's law to capture the bending deformations. Since Eq. (1) shows 1D strain in an equi-biaxial tension test, to convert the 2D area change to 1D extension, a coefficient of 1/2 is multiplied by $(\Delta A/A)$. We also note that Eq. (1) is not a constitutive law but rather a phenomenological model that can capture the geometric nonlinearity of wrinkled membranes during equi-biaxial straining.

As shown in Fig. 1, the typical stress–strain curve of a wrinkled membrane is composed of a linear part $[\varepsilon_L = \left(1/E^f_{2D}\right)\sigma]$ and a nonlinear part $[\varepsilon_{NL} = (1/2)(\Delta A(\sigma)/A)]$, which converges to $(1/2)(\Delta A/A)_{\max}$ at large strains. From Eq. (1), it is then possible to obtain the effective stiffness of the membrane as

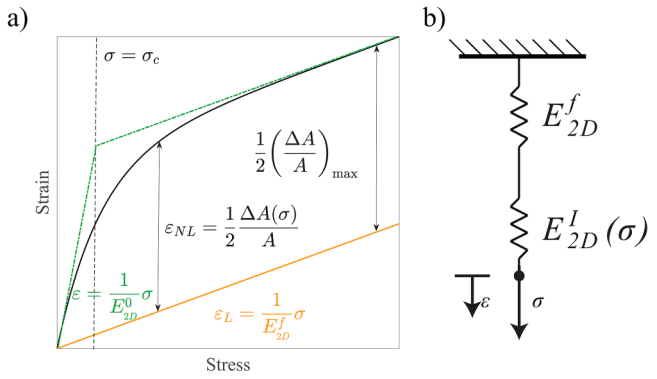

FIG. 1. Phenomenological model of the effective stress–strain response of biaxially tensioned wrinkled graphene membranes. (a) Schematic representation of the bilinear approximation and its independent and dependent parameters. The solid black line is the response of a wrinkled membrane following Eqs. (1)–(3), the solid orange line represents a pristine unwrinkled membrane and the dashed-dotted green lines are the tangents to the curve close to the origin and at maximum stress [bilinear approximation, Eq. (4)]; (b) spring-in-series system with a linear spring with constant stiffness representing the intrinsic stiffness of flat pristine graphene E^f_{2D} and nonlinear spring with a stress-dependent stiffness $E^I_{2D}(\sigma)$ representing the stiffness of the wrinkles.

$$\frac{1}{E_{\text{eff}}} = \frac{d\varepsilon}{d\sigma} = \frac{1}{E^f_{2D}} + \frac{1}{E^I_{2D}(\sigma)}, \tag{2}$$

where $E^I_{2D}(\sigma)$ can be seen as a stress-dependent nonlinear stiffness term that is in series with a linear spring with constant E^f_{2D} [see Fig. 1(b)]. Comparing Eqs. (1) and (2), the hidden area then obeys the following relation:

$$\frac{1}{2}\frac{\Delta A(\sigma)}{A} = \int \frac{1}{E^I_{2D}(\sigma)} d\sigma. \tag{3}$$

Our goal is to find a symbolic function that best represents the hidden area throughout the wrinkle ironing out process. To capture the physics associated with $E^I_{2D}(\sigma)$, we start from the bi-linear model as shown schematically in Fig. 1(a),

$$\varepsilon(\sigma) = \begin{cases} \frac{1}{E^0_{2D}}\sigma, & \sigma \le \sigma_c, \\ \frac{1}{E^f_{2D}}\sigma + \frac{1}{2}\left(\frac{\Delta A}{A}\right)_{\max}, & \sigma_c < \sigma. \end{cases} \tag{4}$$

We note that this model's stress–strain curve has two slopes that are given by the experimentally measurable tangential stiffness E^0_{2D} of the wrinkled state at low stress and the intrinsic biaxial modulus of graphene E^f_{2D} at high stress. The strain-axis-intercept $(\Delta A/A)_{\max}$ of the high stress line can be determined experimentally by analyzing the stress–strain curves of 2D materials and can also be obtained by performing complementary Raman spectroscopy and interferometric profilometry measurements on wrinkled 2D membranes.[26] Therefore, the unknown transition stress σ_c can be

obtained from Eq. (4) and the continuity condition of the stress–strain curve, which results in

$$\sigma_c = \frac{\frac{1}{2}\left(\frac{\Delta A}{A}\right)_{\max} E^0_{2D} E^f_{2D}}{\left(E^f_{2D} - E^0_{2D}\right)}. \tag{5}$$

To estimate the nonlinear spring response corresponding to wrinkle suppression, we replace $(\Delta A/A)$ in Eq. (3) with $(\Delta A/A)_{\max} g(\sigma/\sigma_c)$, where $g(\sigma/\sigma_c)$ is a function that captures the transition between the two linear regions due to the "ironing out" of the wrinkles that will be determined by comparison to MD simulations and experiments in Sec. IV.

III. ATOMISTIC MODELING

MD simulations are found to be a powerful tool for investigating the influence of wrinkles on the mechanics and material properties of 2D materials under different loading conditions.[28–34] Here, to investigate the influence of different wrinkling patterns on the nonlinear mechanics of 2D membranes, we perform MD simulations where we create wrinkles by two means, as shown in Figs. 2(a) and 2(b), respectively. Either we apply external force at the boundary to deform the membrane, generate wrinkles, and subsequently constrain the boundary to preserve them, or we induce crystal defects to obtain out-of-plane imperfections in the absence of boundary force.

In Fig. 2, we detail out the wrinkle creation process in our study. We start by realizing an initial honeycomb square lattice of graphene (200 × 200 Å^2), comprising 15 744 atoms. To simulate clamped boundary conditions, we fix atoms within a range of 5 Å from each edge. We then create the wrinkles by two methods. In the first method, the wrinkles are created by compressing the boundary coordinates by p% $(0.5 \leq p \leq 7)$ in both directions [Fig. 2(aI)] and use different shape functions to displace the atoms in the z-direction as a function of x and y coordinates [see Fig. 2(aII)]. Finally, to have flat smooth boundaries, we project the obtained shape in Fig. 2(aII) on a kernel that suppresses the wrinkles' height toward boundaries [Fig. 2(aIII)]. We label these wrinkled membranes "pre-stressed" samples throughout the article. The details of the wrinkling patterns and the kernel for suppressing boundary wrinkles are given in supplementary material S1.

In the second method, we create stress-free wrinkles using crystal defects, following the procedure mentioned in Ref. 21. Briefly, to achieve this second type of wrinkles, we first arbitrarily select sets of two neighboring atoms (d% of total atoms; $0.5 \leq d \leq 3$) [Fig. 2(bI)] and remove them from the initial lattice [Fig. 2(bII)]. Next, we generate the so-called 5-8-5 defects[21] by creating relevant bonds using Materials Studio software [Fig. 2(bIII)].

The resulting atomic coordinates of wrinkled graphene samples are then used as the input for LAMMPS software.[35] We use Tersoff potential to evaluate atomic interactions.[36] The simulation box walls are built far enough from the graphene edges to avoid numerical interaction between atoms adjacent to the walls, and the boundary conditions are set as periodic. The energy of the

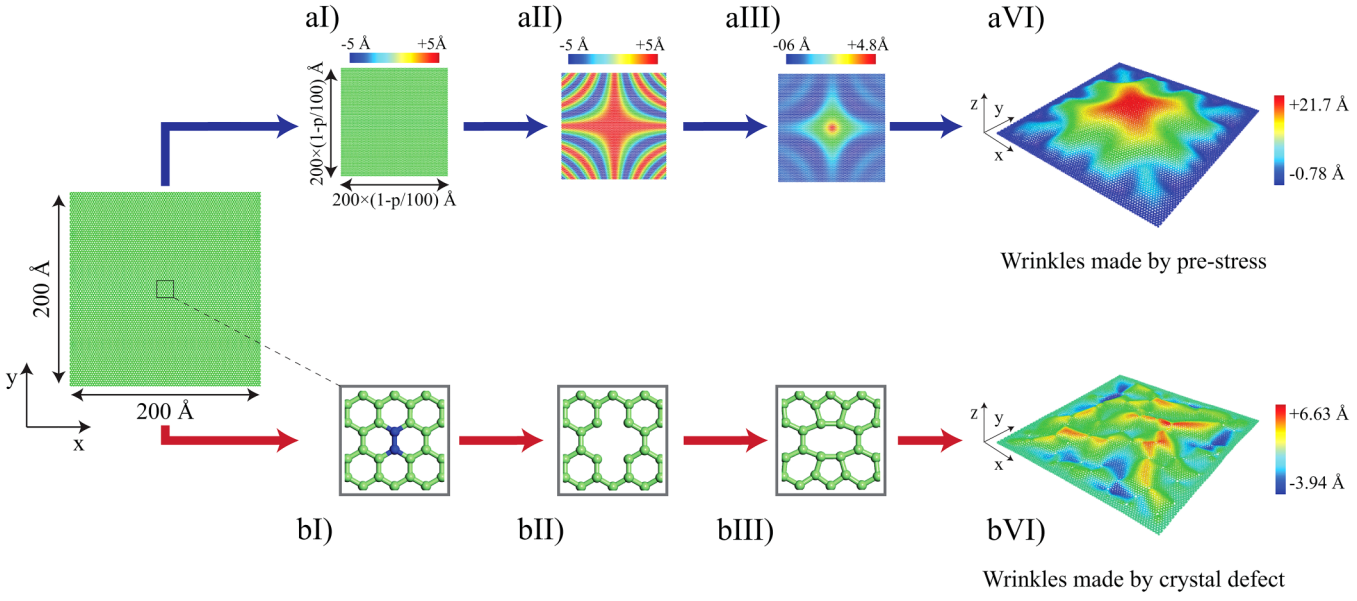

FIG. 2. The procedure for wrinkle creation in MD simulations. (aI) The x and y coordinates are compressed by p%. (aII) Pre-defined shape functions are employed to impose deviation from flat configuration. (aIII) The shape obtained in aII is projected on a Kernel to suppress boundary wrinkles. (aIV) The pre-stressed pattern obtained in LAMMPS after minimizing the energy and thermalizing the system. (bI) Neighboring atoms are randomly chosen and marked through the lattice. (bII) The marked atoms in step bI are removed from the lattice. (bIII) Bonds are created manually, and then the bond angles and lengths are modified locally using Materials Studio software. (bIV) Wrinkled pattern due to crystal defect obtained in LAMMPS after minimizing the energy and thermalizing the system.

system is then minimized with the conjugate-gradient method. To ensure a steady configuration, the created membranes also undergo a canonical ensemble (NVT) for 500 ps. This simulation is carried out using the velocity Verlet integrator with a time step of 1 fs and a Nosé-Hoover thermostat with a time constant of 0.01 ps at 4 K. This relatively low temperature is intentionally chosen to suppress thermodynamical ripples in the lattice,[37] so as to solely study the effect of statically generated wrinkles by pre-stress or crystal defect. We should note that the presence of static wrinkles can mask the influence of thermal ripples. This is mainly because the contraction due to thermal ripples is much smaller than contractions caused by compressive forces at the boundary.[10,26] We should also highlight that $T = 4$ K is chosen over $T = 1$ K merely to decrease computational cost and speed up the thermalization process in the wrinkle creation and equilibration after equi-biaxial loading steps. During the minimization and thermalization of the pre-stressed samples, we fix the boundaries in all directions to prevent the stress release. For the samples with crystal defects, though, we only fix the boundaries in the z-direction and allow movement in x and y to ensure a stress-free configuration. Typical thermalized wrinkled graphene membranes are shown in Figs. 2(aIV) and 2(bIV).

Moreover, to study the effect of both pre-stress and crystal defects simultaneously, we performed additional simulations in which after creating defects, we compressed the samples and then fixed the boundary coordinates in x, y, and z directions. We shall also emphasize that the pre-stressed wrinkles are made only by compression, and the samples are sufficiently equilibrated in LAMMPS to ensure isotropic behavior. Moreover, the location of crystal defects are chosen randomly to avoid possible anisotropy of stress-free wrinkles.

IV. RESULTS AND DISCUSSION

A. MD simulations

To probe the elasticity of the created samples upon biaxial stretching, we apply pseudo-static tensile strains to the four

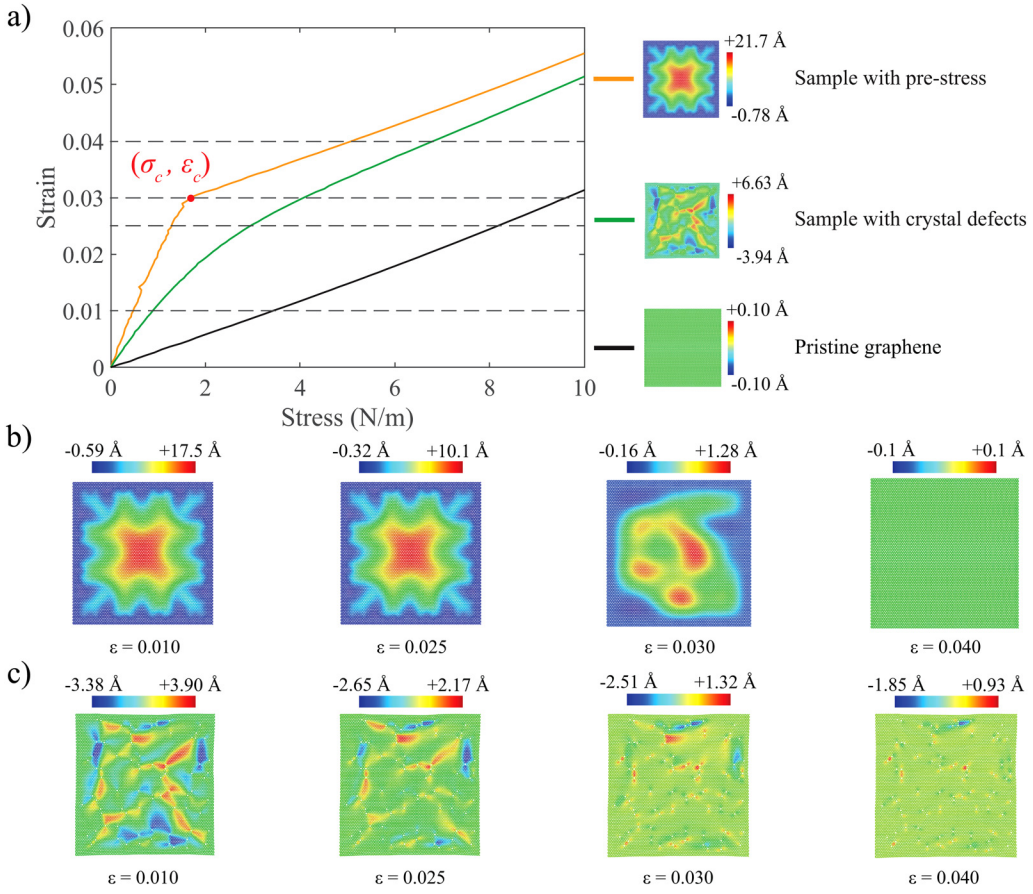

FIG. 3. Biaxial tensile response of wrinkled graphene with pre-stress (achieved by 2.3% compressive force in both x and y-directions) and 5-8-5 crystal defects (achieved by 1% defects): (a) Stress–strain response. Snapshots of the pre-stressed sample upon tension, corresponding to the dashed lines shown in (a), are shown for (b) pre-stressed and (c) stress-free wrinkled sample. The color-scales demonstrate the local height of wrinkles. The orange line represents the sample with pre-stress, and the green line shows the sample with crystal defects. Moreover, the black line despicts pristine graphene data.

boundaries in discrete steps of 0.1 ns (rate of 0.5 Å/ns), with a relaxation period of 0.1 ns. The stepwise strain-increment is repeated many times to achieve stretching in x- and y-directions. The average biaxial stresses are then obtained by calculating the average normal force at the boundaries and dividing it by the perimeter. The tangential biaxial stiffness is merely the slope of the stress–strain curve at every applied strain.

Figure 3(a) shows the stress–strain response of the pre-stressed and defected samples obtained in Fig. 2, along with the elastic response of pristine graphene. We note that the pristine and the defected sample are at their stress-free state at the origin, while the pre-stressed sample is at a compressed state ($p = 2.3$). A linear relationship can be observed between stress and strain for the pristine graphene with a slope of $E^f_{2D} = 330\,\mathrm{N/m}$ that corresponds to the stretching of carbon–carbon bonds. The obtained value of E^f_{2D} matches well the acclaimed high biaxial stiffness of graphene.[38–40] In contrast, for the pre-stressed sample, the stress–strain response is characterized by two slopes, and the sample with crystal defects exhibits nonlinear behavior. We note that the observed nonlinearity is at relatively low strains and is different from the nonlinear response characterized by the negative third-order elastic modulus of graphene.[41,42] The latter nonlinear response comes into play only at high strains.

To understand how wrinkling patterns evolve with the applied strain, in Figs. 3(b) and 3(c), we trace the morphology of our graphene samples while straining them. It is interesting to note that for the pre-stressed sample, the wrinkling shape only changes at a critical strain ε_c associated with critical stress σ_c before which only the height of the created wrinkle shrinks. At ε_c, a change in the wrinkling pattern can be observed in Fig. 3(b). We note that the observed pattern is unstable and with a slight additional strain the membrane flattens completely. However, in the sample with crystal defect [see Fig. 3(c)], even at relatively high strains, e.g., 4%, the sheet still has buckled regions locally. Movies of the MD simulations associated with the stretching process for both samples are shown in supplementary material S2.

To explain the observed morphology change, in Figs. 4(a) and 4(b), we show the average bond length and the average wrinkle height as a function of the applied biaxial strain, respectively. Interestingly, unlike the sample with crystal defects where a nonlinear trend in the average bond length variation is apparent for the pre-stressed sample before the critical strain ε_c, the average bond length is ≈1.46 Å, that is the stable bond length of the Tersoff potential at 4 K. This observation suggests that for the pre-stressed sample beyond ε_c, only the atomic bonds of graphene are being stretched, while before ε_c, graphene is subjected to both in-plane and out-of-plane deformation. A similar conclusion can be drawn by tracing the average wrinkle height of the pre-stressed sample [see Fig. 4(b)], where a gradual decrease can be observed until ε_c, after which the wrinkles are ironed out. It is also apparent from the figures that throughout the straining procedure, pristine graphene stays planar, and its bond length varies linearly as a function of strain.

B. Symbolic regression of MD data

Next, to obtain an analytic expression that captures the observed nonlinearity, we determine $g(\sigma/\sigma_c)$. For this, we convert

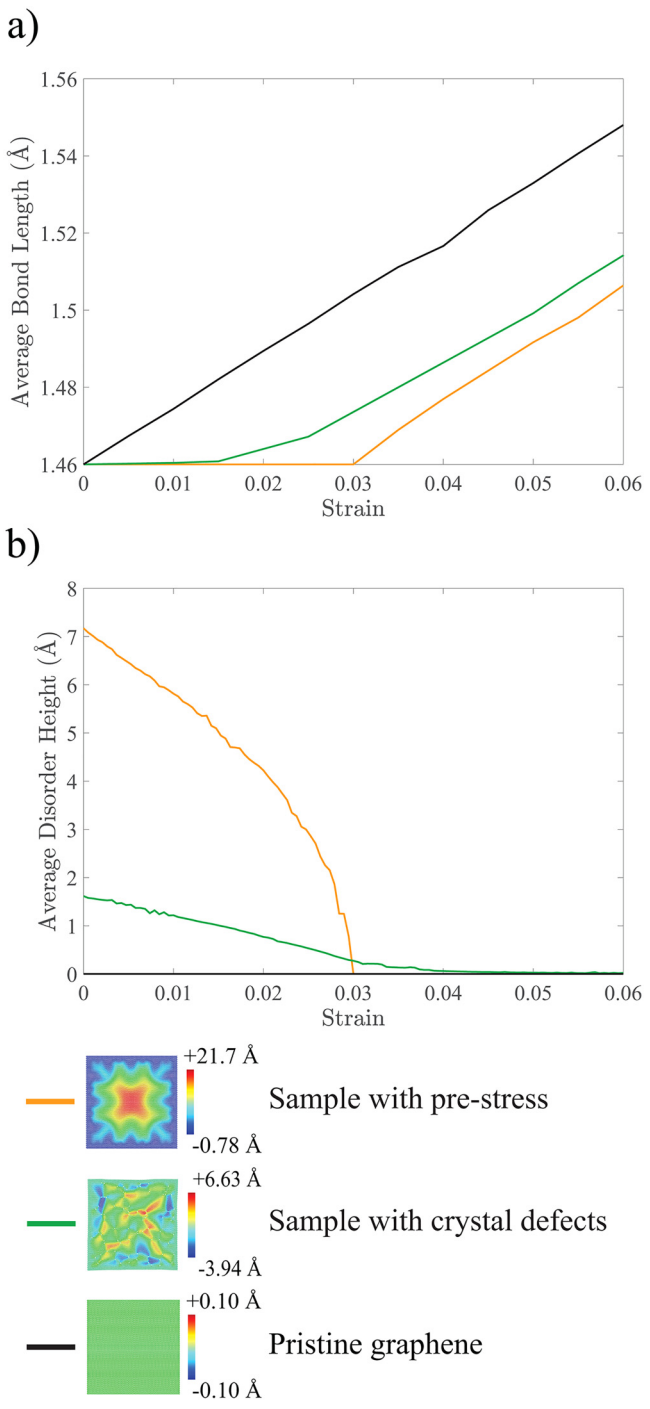

FIG. 4. Average bond length and wrinkle height as a function of strain. (a) Average carbon–carbon bond-length of the samples; (b) average sample height calculated by $\frac{1}{N}\sum_{i=1}^{N}|z_i|$ (N, total number of atoms, z_i, the z-coordinate of the atom i). The color scales demonstrate the local height of wrinkles. The orange line represents the sample with pre-stress, and the green line shows the sample with crystal defects. Moreover, the black line depicts pristine graphene data.

the $\varepsilon(\sigma)$ curves from the MD data into $\Delta A(\sigma)/A$ curves using Eq. (4). By doing so, we can eliminate the contribution of Hooke's law from the datasets and use Eureqa to determine only the hidden area symbolically. We also make the datasets dimensionless by dividing stress by σ_c, and to retain only $g(\sigma/\sigma_c)$ in the fitting procedure, we divide the strain by $(1/2)(\Delta A/A)_{max}$. We obtain the normalized function $g(\sigma/\sigma_c)$ for 38 wrinkling configurations. These patterns include 24 wrinkled membranes with pre-stress created in a similar fashion to Fig. 2(aIV), 10 samples with crystal defects obtained similar to Fig. 2(bIV), and 4 graphene membranes that have both pre-stress and crystal defect (see supplementary material S1). In Fig. 5, we show the normalized response of seven of these membranes, and in Table I, we report the corresponding bi-linear fits using Eq. (4). It is interesting to note that all the samples created by crystal defects follow the same trend of nonlinearity irrespective of the shape and height of wrinkles (samples D, E, and F). The same observation holds true for the samples made by pre-stress (samples A, B, and C) where a bi-linear response is apparent. We note that the stress–strain response of samples with both pre-stress and crystal defects lies within the response of the wrinkled membranes made by crystal defect and those made by pre-stress only (see sample G).

To analytically describe the stress–strain characteristics of membranes with different types of wrinkles, it is thus interesting to obtain a phenomenological equation that can capture all the observed curves $g(\sigma/\sigma_c)$. To this end, we import the normalized stress–strain data $[g(\sigma/\sigma_c)]$ into the Eureqa symbolic regression software to automatically search for a function space using a selected set of operators and operands.[43] Eureqa uses genetic programming to search for mathematical equations that best describe a set of data and has been successfully used to distill physical laws of motion from experimental data.[43,44] The output of Eureqa is a set of possible fitting functions (Pareto front) ranked based on the mean absolute error and a complexity index that balances the complexity of the proposed models, measured as the number of terms included in the model (see supplementary material S3). The obtained models from Eureqa were either overfitting the MD data or contained few fitting parameters. Among the proposed models, the following symbolic function is found to fit both samples with pre-stress and crystal defects with high accuracy:

$$\varepsilon = \frac{1}{E^f_{2D}}\sigma + \frac{1}{2}\left(\frac{\Delta A}{A}\right)_{max}\left[\frac{\sigma/\sigma_c}{\sigma/\sigma_c + \exp\left(-(\sigma/\sigma_c) - \beta(\sigma/\sigma_c)^4\right)}\right]. \quad (6)$$

In this model, the nonlinear spring can be well-approximated by three physically meaningful and measurable parameters, namely, E^f_{2D}, σ_c, and $(\Delta A/A)_{max}$ in addition to the fitting parameter β that determines the degree of nonlinearity. We note that in the limit of $\beta \to 1$, Eq. (6) is seen to represent the response of wrinkled membranes made by pre-stress well, while in the limit of $\beta \to 0.1$, stress-free wrinkled membranes can be best fitted (see Fig. 5). Moreover, we observe that the mechanical response of samples made by a combination of pre-stress and crystal defects can be well-captured by $0.1 < \beta < 1$ (see Table S4 in supplementary material S4). We also note that for $\beta \to -\infty$, the nonlinear term of Eq. (6) tends to zero and Hooke's law is retrieved. The fits to all 38 samples using Eq. (6) are given in supplementary material S4. The presented phenomenological model can capture the nonlinear response of a large set of wrinkled membranes, with functional form being obtained directly from MD fits . It is important to note that there might be wrinkling patterns that cannot be captured by Eq. (6), e.g., wrinkles made by shear. Thus, more MD work will be

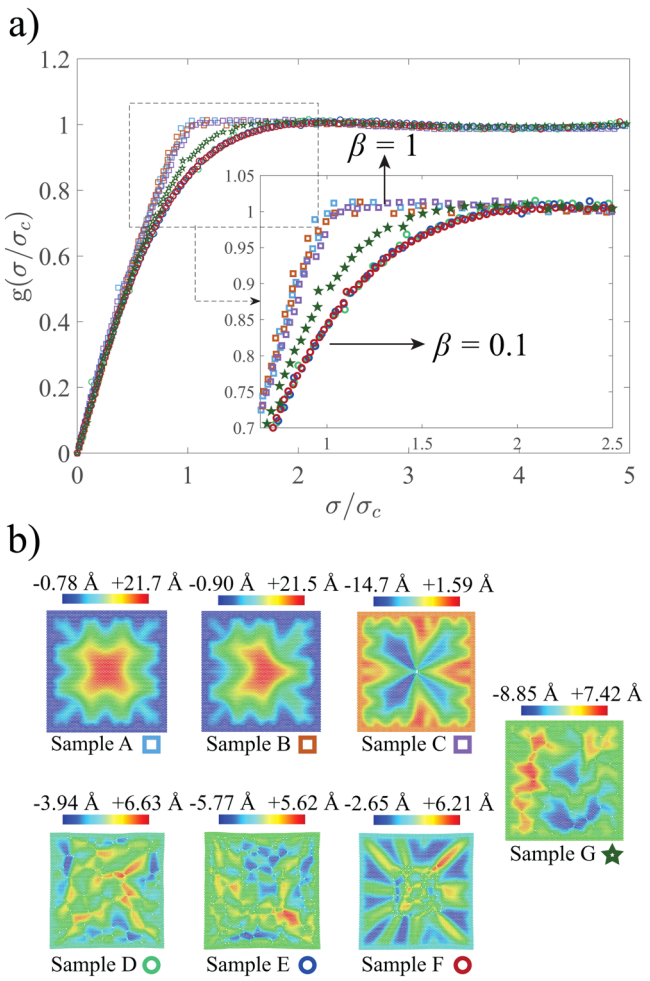

FIG. 5. Uniqueness of degree of nonlinearity for samples with pre-stress and crystal defects. (a) $g(\sigma/\sigma_c)$ for seven different samples: A, B, and C pre-stressed graphene with 2.3%, 2.3%, and 2.1% pre-stress; D and E, graphene with randomly distributed 1% and 2% crystal defects; F, graphene with 1% locally created defects; and G, graphene with 2.1% pre-stress and 0.5% crystal defects. (b) Corresponding graphene samples with different wrinkle types/patterns at the start of stretching. The color-scales demonstrate local wrinkle height and the color symbols shown below each sample represents the corresponding data in (a). The corresponding parameters obtained from MD simulations and used for normalizing the stress–strain data are presented in Table I.

TABLE I. Bilinear approximation [Eq. (4)] parameters corresponding to the samples A-G, explained in Fig. 5.

	E^f_{2D}(N m^{-1})	$(\Delta A/A)_{\max}$	σ_c(N m^{-1})
Sample A	326.3	0.047	1.244
Sample B	332.7	0.046	1.321
Sample C	308.6	0.042	1.971
Sample D	282.5	0.031	1.858
Sample E	258.2	0.045	2.621
Sample F	286.0	0.029	1.941
Sample G	309.3	0.043	1.478

needed to establish the range of validity of the presented phenomenological model.

It is interesting to note that in statistical mechanics studies,[45] there also exists a parameter α that expresses the degree of nonlinearity in wrinkled membranes, and it was shown that in stress-free wrinkled membranes, irrespective of wrinkling pattern, the nonlinear behavior can be modelled as

$$\varepsilon(\sigma) = \frac{1}{E^f_{2D}}\sigma + \frac{\sigma_*}{\alpha E^f_{2D}}\left(\frac{\sigma}{\sigma_*}\right)^{\alpha}, \tag{7}$$

with $\alpha \approx 0.1$ for statically wrinkled membranes, and σ_* being a re-normalization parameter set as the stress at which $E^I_{2D}(\sigma) = E^f_{2D}(\sigma/\sigma_*)^{1-\alpha}$, that is when the nonlinear stiffness of Eq. (7) is equal to the linear stiffness term E^f_{2D}.[45]

It was found that it is difficult to accurately fit the MD data with the physics-based Eq. (7), which is why the phenomenological Eq. (6) is introduced, that matches the MD simulations with high accuracy.

C. Validation of the model using experimental data

In order to show the applicability of Eq. (6) in fitting experimental data and to compare its outcome to Eq. (7), we fit the stress–strain measurements for single-layer graphene membranes reported in Ref. 26 using both Eq. (6) [in Fig. 6(b)] and Eq. (7) [in Fig. 6(a)]. The graphene membranes in the experiments[26] were suspended over 5 μm circular cavities and pressurized by nitrogen gas while their strain was probed by both Raman spectroscopy and interferometric profilometry. Before fitting, first the Raman spectroscopy values for the strain were subtracted from interferometric measurements. Thus, the experimental data of Ref. 26 only contain the nonlinear strain ε_{NL} corresponding to $(1/2)(\Delta A(\sigma)/A)$ [see Fig. 1(a)]. In order to account for the offset seen in the data at the beginning of the measurements, σ and σ_* in Eq. (7) were replaced with $\sigma - \sigma_0$ and $\sigma_* - \sigma_0$, respectively, with σ_0 being an un-known pre-stress. Then, α, σ_*, and σ_0 were chosen as the fitting parameters. The obtained values from the fits in[26] were $\alpha = 0.12 \pm 0.02$, $\sigma_* = 0.8 \pm 0.1$ N/m, and $\sigma_0 = 0.07 \pm 0.01$ N/m.

Although the obtained fits provide good insight and confirm deviation from Hooke's law in wrinkled membranes, it appears that with increasing stress, the fitted curves in Fig. 6(a) deviate from the experimental data. A possible reason for this deviation is that the model proposed in Ref. 45 is derived for membranes that exhibit stress-free out-of-plane fluctuations and does not account for the pre-stress often present after the fabrication of graphene membranes. Another reason might be the finite bending rigidity of graphene which results in the non-zero stiffness that samples show at low stress, before ironing out the wrinkles (see Fig. 6).

For comparison, in Fig. 6(b), we show the fits of experimental data using Eq. (6). To capture the nonlinear behavior, we use

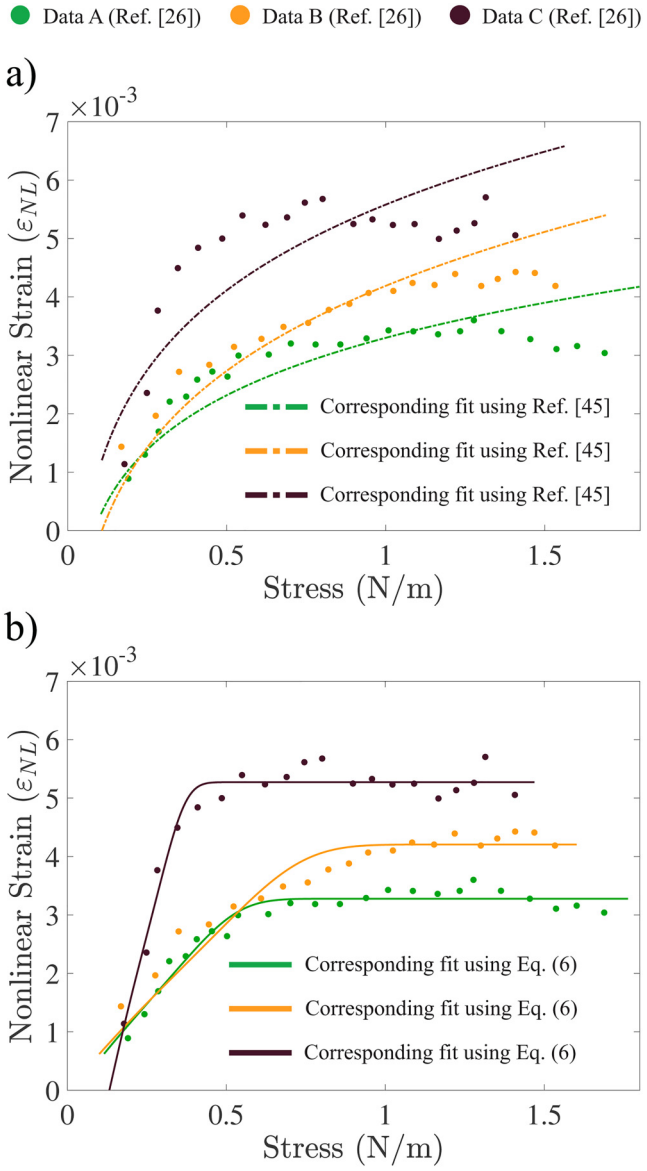

FIG. 6. Fits of the experimental stress–strain data reported in Ref. 26. (a) Fits obtained using the power-law relation proposed by Gornyi *et al.*[45] (b) Curves obtained by fitting the data with [Eq. (6)].

$(\Delta A/A)_{max}$ and σ_c as the fitting parameters and fix $\beta = 1$, that is the degree of nonlinearity obtained from our MD simulations for pre-stressed wrinkled membranes. Similar to the procedure performed in Ref. 26, we also add a constant term σ_0 to Eq. (6) to account for the offset observed at the onset of experiments. Using these fitting parameters, we find $(\Delta A/A)_{max} = 0.008 \pm 0.002$, $\sigma_c = 0.45 \pm 0.2$ N/m, $\sigma_0 = 0.065 \pm 0.065$ N/m and find good fits to the nonlinear stress–strain trends observed experimentally.

It is worth noting that the parameter β is a qualitative measure of the smoothness of the transition between the two straight parts of the stress–strain curve. For $\beta = 1$, this transition is a sharp kink, a situation that corresponds to pre-stressed graphene, whereas for $\beta = 0.1$, the transition is more smooth, a situation that is representative of crystal defect-induced wrinkles. Further theoretical work is required to clarify the physical origin of the proposed functional form for the hidden area of wrinkled 2D materials and the effect of defects and wrinkles on the value of β. Such theoretical work should be carried out using statistical mechanics theory of membranes with crystalline or hexatic order similar to Ref. 45 or 46 accounting for the pre-stress effect. It would be interesting to see if such models obtain a nonlinear function for wrinkle ironing out process similar to our symbolic regression approximation.

We shall stress that the fits presented are aimed at demonstrating that the force-deflection curves of experimental data can be well-captured by the presented phenomenological model; thus, the range of applicability of the model is not limited to MD simulations. However, the fitting values obtained for the experimental data are certainly not comparable to the values obtained for the MD results, especially since the exact experimental wrinkling structure is unknown and different from the MD simulations.

V. CONCLUSIONS

In conclusion, we study the effect of wrinkles on the mechanics of graphene using molecular dynamics simulations and obtain bilinear stress–strain characteristics consisting of two linear regions, a low stress region that is related to the "ironing out" of the wrinkles and a high-stress region that is governed by the intrinsic stiffness of graphene. We show that the type of wrinkles influences the smoothness of the transition between these regions. Although wrinkles created by crystal defects in stress-free membranes result in a smooth and gradual transition, wrinkles generated by pre-stressing of graphene by its edges result in a much sharper transition. To capture and characterize these observations, we present a phenomenological model in terms of physically measurable quantities and a fitting parameter β, which determines the degree of nonlinearity and sharpness of the transition. Using this model, we find that membranes with crystal defects and pre-stress each exhibit their unique degrees of nonlinearity irrespective of their wrinkling patterns. Our results suggest that the proposed model can be potentially used to estimate the type of disorder in suspended 2D material membranes by experimentally probing their nonlinear elasticity.

SUPPLEMENTARY MATERIAL

See the supplementary material for the following: S1, the shape functions and smoothing kernel used in forming the wrinkled graphene and the thermalized samples by LAMMPS; S2, convergence of potential energy of wrinkled samples during equilibration; S3, movies of two equi-biaxial tension tests on two different wrinkled samples; S4, detailed procedure of symbolic regression; and S5, the fitting parameters of all 38 samples.

ACKNOWLEDGMENTS

This project has received funding from European Union's Horizon 2020 research and innovation programme under Grant Agreement Nos. 802093 (ERC starting grant ENIGMA), 785219, and 881603 (Graphene Flagship).

AUTHOR DECLARATIONS

Conflict of Interest

The authors have no conflicts to disclose.

DATA AVAILABILITY

The data that support the findings of this study are available from the corresponding author upon reasonable request.

REFERENCES

[1]L. Yang, T. Niu, H. Zhang, W. Xu, M. Zou, L. Xu, G. Cao, and A. Cao, "Self-assembly of suspended graphene wrinkles with high pre-tension and elastic property," 2D Mater. **4**(4), 041001 (2017).
[2]L. Meng, Y. Li, T. S. Liu, C. Zhu, Q. Y. Li, X. Chen, S. Zhang, X. Zhang, L. Bao, Y. Huang, and F. Xu, "Wrinkle networks in exfoliated multilayer graphene and other layered materials," Carbon **156**, 24–30 (2020).
[3]M. Lanza, Y. Wang, A. Bayerl, T. Gao, M. Porti, M. Nafria, H. Liang, G. Jing, Z. Liu, Y. Zhang, and Y. Tong, "Tuning graphene morphology by substrate towards wrinkle-free devices: Experiment and simulation," J. Appl. Phys. **113**(10), 104301 (2013).
[4]W. Chen, X. Gui, L. Yang, H. Zhu, and Z. Tang, "Wrinkling of two-dimensional materials: Methods, properties and applications," Nanoscale Horizons **4**(2), 291–320 (2019).
[5]F. Guinea, B. Horovitz, and P. Le Doussal, "Gauge fields, ripples and wrinkles in graphene layers," Solid State Commun. **149**(27–28), 1140–1143 (2009).
[6]S. Deng and V. Berry, "Wrinkled, rippled and crumpled graphene: An overview of formation mechanism, electronic properties, and applications," Mater. Today **19**(4), 197–212 (2016).
[7]V. M. Pereira, A. C. Neto, H. Y. Liang, and L. Mahadevan, "Geometry, mechanics, and electronics of singular structures and wrinkles in graphene," Phys. Rev. Lett. **105**(15), 156603 (2010).
[8]W. Gao and R. Huang, "Thermomechanics of monolayer graphene: Rippling, thermal expansion and elasticity," J. Mech. Phys. Solids **66**, 42–58 (2014).
[9]S. Lee, "Effect of intrinsic ripples on elasticity of the graphene monolayer," Nanoscale Res. Lett. **10**(1), 1–9 (2015).
[10]R. J. Nicholl, H. J. Conley, N. V. Lavrik, I. Vlassiouk, Y. S. Puzyrev, V. P. Sreenivas, S. T. Pantelides, and K. I. Bolotin, "The effect of intrinsic crumpling on the mechanics of free-standing graphene," Nat. Commun. **6**(1), 1–7 (2015).
[11]B. Rakshit and P. Mahadevan, "Absence of rippling in graphene under biaxial tensile strain," Phys. Rev. B **82**(15), 153407 (2010).
[12]A. Fasolino, J. H. Los, and M. I. Katsnelson, "Intrinsic ripples in graphene," Nat. Mater. **6**(11), 858–861 (2007).
[13]B. Sajadi, S. Wahls, S. van Hemert, P. Belardinelli, P. G. Steeneken, and F. Alijani, "Nonlinear dynamic identification of graphene's elastic modulus via reduced order modeling of atomistic simulations," J. Mech. Phys. Solids **122**, 161–176 (2019).

[14]H. Vandeparre, M. Piñeirua, F. Brau, B. Roman, J. Bico, C. Gay, W. Bao, C. N. Lau, P. M. Reis, and P. Damman, "Wrinkling hierarchy in constrained thin sheets from suspended graphene to curtains," Phys. Rev. Lett. **106**(22), 224301 (2011).
[15]S. D. Janssens, B. Sutisna, A. Giussani, J. A. Kwiecinski, D. Vázquez-Cortés, and E. Fried, "Boundary curvature effect on the wrinkling of thin suspended films," Appl. Phys. Lett. **116**(19), 193702 (2020).
[16]D. T. Ho, H. S. Park, S. Y. Kim, and U. Schwingenschlogl, "Graphene origami with highly tunable coefficient of thermal expansion," ACS Nano **14**(7), 8969–8974 (2020).
[17]S. Zhao, Y. Zhang, J. Yang, and S. Kitipornchai, "Significantly improved interfacial shear strength in graphene/copper nanocomposite via wrinkles and functionalization: A molecular dynamics study," Carbon **174**, 335–344 (2021).
[18]Z. F. Wang, Y. Zhang, and F. Liu, "Formation of hydrogenated graphene nanoripples by strain engineering and directed surface self-assembly," Phys. Rev. B **83**(4), 041403 (2011).
[19]D. Akinwande, C. J. Brennan, J. S. Bunch, P. Egberts, J. R. Felts, H. Gao, R. Huang, J. S. Kim, T. Li, Y. Li, and K. M. Liechti, "A review on mechanics and mechanical properties of 2D materials—Graphene and beyond," Extreme Mech. Lett. **13**, 42–77 (2017).
[20]H. Qin, Y. Sun, J. Z. Liu, and Y. Liu, "Mechanical properties of wrinkled graphene generated by topological defects," Carbon **108**, 204–214 (2016).
[21]J. N. Grima, S. Winczewski, L. Mizzi, M. C. Grech, R. Cauchi, R. Gatt, D. Attard, K. W. Wojciechowski, and J. Rybicki, "Tailoring graphene to achieve negative Poisson's ratio properties," Adv. Mater. **27**(8), 1455–1459 (2015).
[22]D. Yoon, Y. W. Son, and H. Cheong, "Negative thermal expansion coefficient of graphene measured by Raman spectroscopy," Nano Lett. **11**(8), 3227–3231 (2011).
[23]M. I. Katsnelson and A. Fasolino, "Graphene as a prototype crystalline membrane," Acc. Chem. Res. **46**(1), 97–105 (2013).
[24]B. Sajadi, S. van Hemert, B. Arash, P. Belardinelli, P. G. Steeneken, and F. Alijani, "Size-and temperature-dependent bending rigidity of graphene using modal analysis," Carbon **139**, 334–341 (2018).
[25]K. Cao, S. Feng, Y. Han, L. Gao, T. H. Ly, Z. Xu, and Y. Lu, "Elastic straining of free-standing monolayer graphene," Nat. Commun. **11**(1), 284 (2020).
[26]R. J. Nicholl, N. V. Lavrik, I. Vlassiouk, B. R. Srijanto, and K. I. Bolotin, "Hidden area and mechanical nonlinearities in freestanding graphene," Phys. Rev. Lett. **118**(26), 266101 (2017).
[27]C. H. Yoo and S. Lee, *Stability of Structures: Principles and Applications* (Elsevier, 2011).
[28]J. A. Baimova, S. V. Dmitriev, K. Zhou, and A. V. Savin, "Unidirectional ripples in strained graphene nanoribbons with clamped edges at zero and finite temperatures," Phys. Rev. B **86**(3), 035427 (2012).
[29]M. Neek-Amal and F. M. Peeters, "Graphene nanoribbons subjected to axial stress," Phys. Rev. B **82**(8), 085432 (2010).
[30]J. A. Baimova, S. V. Dmitriev, and K. Zhou, "Strain-induced ripples in graphene nanoribbons with clamped edges," Phys. Status Solidi B **249**(7), 1393–1398 (2012).
[31]W. H. Duan, K. Gong, and Q. Wang, "Controlling the formation of wrinkles in a single layer graphene sheet subjected to in-plane shear," Carbon **49**(9), 3107–3112 (2011).
[32]N. Jing, Q. Xue, C. Ling, M. Shan, T. Zhang, X. Zhou, and Z. Jiao, "Effect of defects on Young's modulus of graphene sheets: A molecular dynamics simulation," RSC Adv. **2**(24), 9124–9129 (2012).
[33]L. He, S. Guo, J. Lei, Z. Sha, and Z. Liu, "The effect of Stone–Thrower–Wales defects on mechanical properties of graphene sheets: A molecular dynamics study," Carbon **75**, 124–132 (2014).
[34]J. M. Leyssale and G. L. Vignoles, "A large-scale molecular dynamics study of the divacancy defect in graphene," J. Phys. Chem. C **118**(15), 8200–8216 (2014).
[35]S. Plimpton, "Fast parallel algorithms for short-range molecular dynamics," J. Comput. Phys. **117**(1), 1–19 (1995).
[36]J. J. P. R. B. Tersoff, "Modeling solid-state chemistry: Interatomic potentials for multicomponent systems," Phys. Rev. B **39**(8), 5566 (1989).
[37]Y. Zhang and L. Wang, "Thermally stimulated nonlinear vibration of rectangular single-layered black phosphorus," J. Appl. Phys. **124**(13), 135101 (2018).
[38]K. N. Kudin, G. E. Scuseria, and B. I. Yakobson, "C 2 F, BN, and C nanoshell elasticity from *ab initio* computations," Phys. Rev. B **64**(23), 235406 (2001).
[39]D. Davidovikj, F. Alijani, S. J. Cartamil-Bueno, H. S. van der Zant, M. Amabili, and P. G. Steeneken, "Nonlinear dynamic characterization of two-dimensional materials," Nat. Commun. **8**(1), 1–7 (2017).
[40]B. Sajadi, F. Alijani, D. Davidovikj, J. Goosen, P. G. Steeneken, and F. van Keulen, "Experimental characterization of graphene by electrostatic resonance frequency tuning," J. Appl. Phys. **122**(23), 234302 (2017).
[41]E. Cadelano, P. L. Palla, S. Giordano, and L. Colombo, "Nonlinear elasticity of monolayer graphene," Phys. Rev. Lett. **102**(23), 235502 (2009).
[42]C. Lee, X. Wei, J. W. Kysar, and J. Hone, "Measurement of the elastic properties and intrinsic strength of monolayer graphene," Science **321**(5887), 385–388 (2008).
[43]M. Schmidt and H. Lipson, "Distilling free-form natural laws from experimental data," Science **324**(5923), 81–85 (2009).
[44]J. Bongard and H. Lipson, "Automated reverse engineering of nonlinear dynamical systems," Proc. Natl. Acad. Sci. U.S.A. **104**(24), 9943–9948 (2007).
[45]I. V. Gornyi, V. Y. Kachorovskii, and A. D. Mirlin, "Anomalous Hooke's law in disordered graphene," 2D Mater. **4**(1), 011003 (2016).
[46]R. Roldán, A. Fasolino, K. V. Zakharchenko, and M. I. Katsnelson, "Suppression of anharmonicities in crystalline membranes by external strain," Phys. Rev. B **83**(17), 174104 (2011).